Cryptic metasomatism revealed by Li isotopes of mantle xenoliths beneath Thrace Basin, NW Turkey

Jie-Jun Jing, Ben-Xun Su, Yan Xiao, Laure Martin, Hong-Fu Zhang, İbrahim Uysal, Chen Chen, Wei Lin, Yang Chu, Hans-Michael Seitz, Peng-Fei Zhang

PII: S1367-9120(18)30366-3
DOI: https://doi.org/10.1016/j.jseaes.2018.08.025
Reference: JAES 3629

To appear in: *Journal of Asian Earth Sciences*

Received Date: 9 July 2018
Revised Date: 25 August 2018
Accepted Date: 25 August 2018

Please cite this article as: Jing, J-J., Su, B-X., Xiao, Y., Martin, L., Zhang, H-F., Uysal, I., Chen, C., Lin, W., Chu, Y., Seitz, H-M., Zhang, P-F., Cryptic metasomatism revealed by Li isotopes of mantle xenoliths beneath Thrace Basin, NW Turkey, *Journal of Asian Earth Sciences* (2018), doi: https://doi.org/10.1016/j.jseaes.2018.08.025

Cryptic metasomatism revealed by Li isotopes of mantle xenoliths beneath Thrace Basin, NW Turkey

Jie-Jun Jing [1, 2, 3*], Ben-Xun Su [1, 2*], Yan Xiao [3], Laure Martin [4], Hong-Fu Zhang [2, 3], İbrahim Uysal [5], Chen Chen [1, 2], Wei Lin [2, 3], Yang Chu [2, 3], Hans-Michael Seitz [6], Peng-Fei Zhang[7]

[1] Key Laboratory of Mineral Resources, Institute of Geology and Geophysics, Chinese Academy of Sciences, Beijing 100029, China

[2] University of Chinese Academy of Sciences, Beijing 100049, China

[3] State Key Laboratory of Lithospheric Evolution, Institute of Geology and Geophysics, Chinese Academy of Sciences, P.O. Box 9825, Beijing 100029, China

[4] Centre for Microscopy, Characterisation and Analysis, University of Western Australia, Crawley, WA 6009, Australia

[5] Department of Geological Engineering, Karadeniz Technical University, 61080-Trabzon, Turkey

[6] Goethe-Universität Frankfurt, Altenhöferallee 1, Frankfurt am Main, Germany

[7] Department of Earth Science, The University of Hong Kong, Hong Kong, China

Abstract

To identify metasomatic overprints in the mantle xenoliths from Tethys orogenic belt in NW Turkey, we report here *in situ* Li concentrations and isotopic compositions of olivine, clinopyroxene and orthopyroxene along with major element compositions

* Corresponding authors: Jie-Jun Jing, jjjing@mail.iggcas.ac.cn; Ben-Xun Su, subenxun@mail.iggcas.ac.cn.

of minerals, and bulk rock trace element compositions of the mantle xenoliths composed of refractory harzburgites with subordinate lherzolites and one olivine-websterite. Their non-depleted bulk rock light rare earth element (LREE) patterns, enrichment in large ion lithophile elements and depletion of high field strength elements, imply subduction-related metasomatism, while the Y-depletion may indicate the derivation of the metasomatic melts/fluids from a garnet-bearing source. Minerals from all the xenoliths display homogeneous major element compositions, however they show large intra- and inter-mineral Li elemental and isotopic variations. The Li contents of olivines range from 1.45 to 2.81 ppm with large variations in δ^7Li values (+1.2 to +17.5‰). The orthopyroxenes have variable Li contents (0.07 to 16.6 ppm) and δ^7Li values (-71.6 to +10.8‰), with higher Li contents and lower δ^7Li values in their cores. The clinopyroxenes show variable Li contents (2.16-22.0 ppm) and δ^7Li values (-54.6 to +1.9‰), with commonly higher Li contents and lower δ^7Li values in their cores. The Li-isotopic zonation observed in most pyroxene grains is most likely a recent overprint of subduction-related fluids. In contrast, olivines with fairly homogeneous low Li contents compared to pyroxenes appear to be less affected by the metasomatic fluids/melts. The correlation between δ^7Li values and the forsterite contents of olivines, along with the preferential uptake of Li in pyroxenes, and the presence of light Li isotopic compositions in the cores of pyroxenes, indicate the influence of silicate melt-rock interaction. We interpret these results as evidence for a metasomatic overprint predating the zonation in the Tethys orogenic belt of NW Turkey. Thus, both the recent fluid metasomatism and earlier silicate melt metasomatism are strongly related with the successive subduction of the Tethyan oceanic plate.

Keywords: Li isotopes; Mantle xenolith; Mantle metasomatism; Tethyan ocean,

Turkey

1. Introduction

Mantle metasomatism plays a critical role in modifying the chemical properties of the lithospheric mantle. Metasomatism can be divided into two types, namely, modal and cryptic metasomatism (Harte et al., 1983; Dawson et al., 1984). Dykes, melt veins, and the presence of secondary garnet, clinopyroxene and/or amphibole in peridotites, are evidences for modal metasomatism (Menzies et al., 1987; Wilkinson and Maitre, 1987; Green et al., 1988; Prouteau et al., 2001; Ionov et al., 2010), while cryptic metasomatism in peridotites is more difficult to identify as geochemical modifications occur without apparent mineralogical or textural features (Zhang et al., 2002; Rudnick et al., 2004; Menzies et al., 2007; Zhang et al., 2008; Tang et al., 2013). Modified elemental concentration, incompatible trace element enrichment or distinct isotope signatures may be indicative of melt-rock interactions (Dawson et al., 1984; Menzies et al., 1987). However, trace element patterns alone can rarely pinpoint the sources of the metasomatized melts/fluids, because similar chemical signatures can be interpreted as either source characteristics or as a consequence of fractionation during metasomatic processes (Bodinier et al., 1990). For example, it is more difficult to constrain metasomatizing agents and their origin in refractory harzburgites or peridotites which have undergone multi-stages of cryptic metasomatism. Nonetheless, the application of *in situ* Li isotope analysis may provide solutions to this problem due to its capability to detect elemental and isotopic heterogeneities at high spatial resolution (e.g. Seitz and Woodland, 2000; Tang et al., 2007).

The large mass difference (~16%) between the two stable isotopes of Li (^{6}Li and ^{7}Li) leads to strong isotopic fractionation (-20 to +40‰) during many geological

processes (Tomascak, 2004; Jeffcoate et al., 2007). Equilibrium fractionation of Li isotopes is likely to be negligible at high T/P mantle conditions (Tomascak et al., 1999; Magna et al., 2006; Jeffcoate et al., 2007), and Li isotopic heterogeneity could survive 1-2 billion years (Vlastélic et al., 2009). Therefore, Li isotopes have recently become potential geochemical tracers employed to investigate mantle metasomatism (Magna et al., 2008; Zhang et al., 2010; Su et al., 2012). Several studies on peridotites have proposed that Li elemental and isotopic compositions show distinct characteristics and partition behaviors during different kinds of metasomatism (e.g. Seitz and Woodland, 2000; Ottolini et al., 2004; Woodland et al., 2004; Tang et al., 2007; Wagner and Deloule, 2007; Su et al., 2014a). In particular, Li preferentially partitions into pyroxene compared to olivine during silicate metasomatism, whereas it becomes enriched in olivine over pyroxene during carbonatite metasomatism. Moreover, Li isotopes are also indicative of recycling process during subduction (Chan et al., 1999; Elliott et al., 2004, 2006; Marschall et al., 2007). Furthermore, Li is a fast diffusive, fluid mobile element and therefore, elemental and isotopic fractionations of Li are very sensitive to melts/fluids-rock interactions and may record brief and late metasomatic overprints. Thus, Li isotopes may allow us to better understand the evolution of the lithospheric mantle in a subduction environment.

In this study, we present Li isotopic compositions of minerals from a suite of mantle xenoliths (mainly harzburgites) from the Thrace Basin in NW Turkey, determined by in situ analyses using Secondary Ion Mass Spectroscopy (SIMS). We use the extreme Li elemental and Li isotopic variability, present in the various minerals of this suite, to attempt to unravel the nature and timing of the different metasomatic overprints.

2. Geological background and sample descriptions

Turkey consists of several continental fragments joined together into a single landmass in the Miocene (Okay, 2008). The tectonic evolution of Turkey has been influenced by successive subduction of Paleo- and Neo-Tethyan ocean during the convergence between Gondwana and Laurasia (Şengör, 1987; Okay, 1996). The ophiolites of Paleo-Tethyan ocean in Turkey were almost eliminated by continuous tectonic activities, but the Triassic eclogites found in the south of Marmara Sea recorded the subduction of Paleo-Tethyan ocean (Fig. 1b; Okay et al., 1997, 2002). Compared to the Paleo-Tethys, the Neo-Tethyan ocean residues, such as the ophiolites along the Izmir-Ankara suture, are distributed over entire Turkey (Fig. 1a; Emre et al., 1998; Gürbüz and Gürer, 2008a, b). To the north of the Izmir-Ankara suture, late Cretaceous arc volcanic rocks and porphyry copper deposits are widespread in the Strandja Massif and to the north of it (Fig. 1b; Ohta et al., 1988; Öngen, 2000; Karacık et al., 2010). During the Neo-Tethys period, the Thrace Basin evolved as a fore-arc basin, linked to the subduction of the Intra-Pontide ocean (Görür et al., 1996), while the Black Sea Basin in the north developed as an oceanic back-arc basin (Görür, 1988; Okay, 2008). In the Cenozoic, the widespread and active volcanism, namely Hisarlıdağ volcanism, started in the Thrace Basin (Yılmaz and Polat, 1998; Kaymakçı et al., 2007). The Miocene fine-grained basanites and alkali basalts (11.68 ± 0.25 to 8.03 ± 0.19 Ma; Ercan et al., 1995; Aldanmaz et al., 2000) from the Thrace volcanic field contain large amounts of mantle-derived peridotite xenoliths (Fig. 1b, Aldanmaz et al., 2005, 2006; Kaymakçı et al., 2007).

In this study, a suite of mantle xenoliths was collected from the Thrace Basin. The contacts of these xenoliths (up to 30-40 cm in diameter) with the host magma are fairly sharp (Fig. 2a). These xenoliths are all spinel facies and consist predominantly of harzburgites, minor lherzolites and one olivine-websterite. In order to exclude or

minimize diffusional exchange and Li isotope fractionation between xenolith and host lava, the analyzed specimens were selected from the central portion of each xenoliths.

2.1 Harzburgite

The harzburgite samples are commonly medium-grained rocks with protogranular texture (Fig. 2b). They are composed predominantly of olivine (60~80%), orthopyroxene (10~35%) and subordinate clinopyroxene (< 5%), with dark-brown spinel (1~2%) as accessory minerals. Most of the silicate minerals show undulated boundaries, coexisting with fine-grained spinel (Fig. 2h). The olivine grain displays kink band texture (Fig. 2e), whereas the clinopyroxene and spinel lamellae are commonly observed in the orthopyroxenes.

2.2 Lherzolite

The lherzolites are also medium-grained with protogranular texture (Fig. 2c). The typical mineral assemblage of the lherzolites consist of olivine (60~70%), orthopyroxene (25~30%), clinopyroxene (5~10%), and spinel (< 5%). Coarse-grained and granular olivines coexist with medium-grained pyroxenes and fine-grained spinels (Fig. 2g). Orthopyroxene lamellae are common in the clinopyroxenes.

2.3 Olivine-websterite

This is the first olivine-websterite to be found in NW Turkey. It is medium-grained with protogranular texture and curved grain boundaries (Figs. 2d, f). The minerals are orthopyroxene (50~60%), clinopyroxene (~20%), olivine (~30%) and minor spinel (~5%). Clinopyroxene lamellae are observed in orthopyroxene, as well as orthopyroxene lamellae in clinopyroxene.

3. Analytical techniques

3.1 Sample preparation

For EMPA and SIMS measurements, olivine, clinopyroxene and orthopyroxene

separates were handpicked under binocular microscope, and mounted in epoxy together with matrix-matched standards for *in situ* measurements. The mounts were then polished and minerals were characterized by transmitted and reflected light. Optical microscope images of all the minerals served for navigation and identification. For comparison, thin sections of samples BK15-19, BK15-21, BK15-27 and BK15-35 were used for analyses. Mounts and thin sections were carbon-coated for EPMA analyses and gold-coated for SIMS.

3.2 Major elements

Major element compositions of minerals were determined by wavelength dispersive spectrometry using a JEOL JXA8100 electron probe microanalyzer at the Institute of Geology and Geophysics, Chinese Academy of Sciences (IGGCAS). Operating conditions were 15 kV accelerating voltage, 10 nA beam current, 5 μm beam spot and 10-30 s counting time on peak. Natural minerals (jadeite [$NaAlSiO_4$] for Na, Al and Si, rhodonite [$MnSiO_3$] for Mn, sanidine [$KAlSi_3O_8$] for K, garnet [$Fe_3Al_2Si_3O_{12}$] for Fe, Cr-diopside [$(Mg, Cr)CaSi_2O_6$] for Ca, olivine [$(Mg, Fe)_2SiO_4$] for Mg) and synthetic minerals (rutile for Ti, 99.7% Cr_2O_3 for Cr, Ni_2Si for Ni) were used for standard calibration. A program based on the ZAF procedure was used for matrix corrections. Typical analytical uncertainties for all the elements analyzed are better than 1.5%. Mineral major elements data are reported in Supplementary Table S1.

3.3 Li isotopes

Lithium content and isotopic ratio were determined using a Cameca IMS 1280HR SIMS at IGGCAS. Well-characterized natural minerals, namely, olivine (06JY31OL) with fosterite content (Fo=100×Mg/(Mg+Fe)) of 91.2, clinopyroxene (06JY29CPX) with Mg# of 91.9 and orthopyroxene (06JY31OPX) with Mg# of 90.8

(Su et al., 2015), that have compositions similar to those of analyzed minerals, served as standards for the analysis. The O^- primary ion beam was accelerated at 13 kV, with an intensity of 15 to 30 nA. The elliptical spot was approximately 20 × 30 μm in size. Positive secondary ions were measured on an ion multiplier in pulse counting mode, with a mass resolution (M/DM) of 1500 and an energy slit open at 40 eV without any energy offset. A 180-second pre-sputtering without raster was applied before analysis. The secondary ion beam position in the contrast aperture, as well as the magnetic field and the energy offset, was automatically centered before each measurement. Eighty cycles were measured with counting times of 7 and 2 seconds for ^{6}Li and ^{7}Li, respectively. The measured δ^7Li values are given as δ^7Li ($[(^7Li/^6Li)_{sample}/(^7Li/^6Li)_{L\text{-}SVEC}-1] \times 1000$) relative to units of the standard NIST SRM 8545 (L-SVEC) with ^{7}Li /^{6}Li of 12.0192 (Flesch et al., 1973). The olivine standard (06JY31OL) has Li content of 2.70 ± 0.60 ppm with δ^7Li of 4.51 ± 0.33‰, the clinopyroxene standard (06JY29CPX) with Li content of 1.03 ± 0.24 ppm shows δ^7Li of -2.56 ± 0.53‰ and the orthopyroxene standard (06JY31OPX) has Li content of 1.33 ± 0.24 ppm with δ^7Li of -0.19 ± 0.21‰ (Su et al., 2015). The instrumental mass fractionation (IMF) is expressed in δ^7Li units: $\triangle i = \delta^7Li_{SIMS} - \delta^7Li_{MC\text{-}ICPMS}$. The matrix effect, of which δ^7Li increased by 1.0‰ for each mole percent decrease in Fo content of olivine (Su et al., 2015), was considered for calibration. The Li isotopes data are reported in Supplementary Table S1.

3.4 Whole-rock trace elements

Whole-rock trace elements were determined by inductively coupled plasma mass spectrometry, using an Agilent 7500a system at IGGCAS. Whole-rock powders (40 mg, 200 mesh) were dissolved in distilled HF + HNO_3 in Teflon beakers at 200 °C for

5 days, dried, and then digested with HNO_3 at 150 °C for 1 day, and the final step was repeated. International and Chinese standards (BCR-2, BHVO-2, GSR-1, and AGV-2) were used for monitoring drift in mass response during the measurements. The relative error of the ICP-MS analyses was generally better than 5% for most trace elements. Whole-rock trace element data are reported in Supplementary Table S2.

4. Results

4.1 Mineral chemistry and Li isotopes

4.1.1 Olivine

The studied olivines have homogeneous major element compositions. Their Fo contents range from 89.5 to 91.4 in harzburgites, from 89.2 to 90.8 in the lherzolites and from 88.7 to 89.0 in the olivine-websterite. Lithium contents and isotopic compositions of the olivines, show distinct variations. Their Li concentrations vary from 1.45 to 2.82 ppm, mostly within the normal mantle range (1-2 ppm) (an unmetasomatized mantle, Seitz and Woodland, 2000). Lithium isotopic compositions are highly variable, with δ^7Li values of +1.2 to +17.5‰ (Fig. 5a). The δ^7Li values in the olivines are negatively correlated with the Fo contents (Fig. 6a).

4.1.2 Orthopyroxene

In general, the orthopyroxenes display limited major element variations except variable Al_2O_3 (1.93-5.53 wt.%) and CaO (0.33-1.29 wt.%) contents. Their Mg#s vary from 89.2 to 91.7 and are negatively correlated with Al_2O_3 (Fig. 3). Lithium concentrations in the orthopyroxenes are highly variable, ranging from 0.07 to 16.6 ppm. The highest values are recorded in the core of grains (up to 16.6 ppm in sample BK15-9). Analytical spots in some grains show low Li concentrations (<1 ppm) in both refractory harzburgites and fertile lherzolites (e.g. BK15-12, BK15-35, Fig. 5b). Lithium isotopic compositions of the orthopyroxene are extremely variable ranging

from -71.6 to +10.8‰. Almost all the orthopyroxene grains exhibit distinct zonation patterns from core to rim, with higher Li and lighter isotope contents in the cores than the rims (Fig. 7b). Neither Li concentrations nor δ^7Li values are correlated with major elements (Fig. 6b).

4.1.3 Clinopyroxene

Clinopyroxene has the highest Mg# in the range of 90.5 to 93.4 and high CaO contents (19.8-23.6 wt.%) and Al_2O_3 contents (2.42-7.18 wt.%). There is a negative correlation between Mg# and Al_2O_3 (Fig. 3b). Compared to orthopyroxene, the clinopyroxene grains have similarly variable and overall higher Li contents (2.16-22.0 ppm), while the δ^7Li values range from -54.6 to +1.9‰. A general trend from lower δ^7Li in the core to higher δ^7Li in the rim is evident in most clinopyroxenes. However, variations in Li concentrations in clinopyroxene do not reveal a consistent trend with the Li isotopic compositions, as it is for orthopyroxene (Fig. 7). There is also no apparent correlation between the major elements, Li concentrations and Li isotopic compositions (Figs. 5c, 6c).

4.2 Whole-rock trace elements

The harzburgites display variable trace element patterns which are mainly characterized by depleted or flat light rare earth elements (LREE) (Fig. 4a). The lherzolites and the olivine-websterite show depleted LREE patterns (Fig. 4c). Nearly all the samples have slight depletions in the high field strength elements (HFSE) and positive anomalies in large ion lithophile elements (LILE) (Figs. 4b, d). The trace element contents of the harzburgites are generally lower than those of the primitive mantle, while the lherzolites and olivine-websterite trace elements contents are slightly lower or equal to those of the primitive mantle (Figs. 4b, d). Limited range of whole-rock Li contents are recorded in the harzburgite (1.41-1.92 ppm), lherzolite

(1.48-2.37 ppm), olivine-websterite (2.41 ppm), all of which are quite close to that of the upper mantle (< 2 ppm, Tomascak et al., 2016).

5. Discussion

5.1 Origin of lithospheric mantle beneath the Thrace Basin

Aldanmaz et al. (2005) reported the whole rock and mineral geochemical data of the mantle xenoliths from the Thrace Basin and proposed that the mainly refractory harzburgites as well as, the more refractory dunites are residues after melt extraction. The high Fo contents in olivines (~90.0) and the lower whole-rock REE contents (compared to primitive mantle), observed in samples from this study, indicate a partial melting origin. The negative correlation between Mg# and Al_2O_3 in pyroxenes (Fig. 3) confirms the significant partial melting. Olivines in the harzburgites have higher Fo contents than those in the lherzolites and olivine-websterite, consistent with higher degrees of melt extraction within the harzburgites. However, the lherzolite and the olivine-websterite are more depleted in LREE than some refractory harzburgites but no accessory minerals, such as amphibole or phlogopite were observed in the harzburgite (Fig. 4), which is inconsistent with melt extraction. The flat REE patterns of the harzburgites are also inconsistent with their formation as single-stage melting residues of a fertile source, indicating the occurrence of cryptic metasomatism.

5.2 Li diffusion

The minerals investigated in this study display large Li elemental and isotopic heterogeneity within and between grains. (Figs. 5, 7). Because Li diffusive rate is slower in olivine than in clinopyroxene and ^{6}Li diffuses faster than ^{7}Li (Richter et al., 2003; Coogan et al., 2005; Lundstrom et al., 2005), light Li isotope signatures in clinopyroxene and heavy Li isotopic compositions in olivine in mantle xenoliths, have generally been explained by prolonged cooling upon eruption (Coogan et al., 2005;

Ionov and Seitz, 2008; Gao et al., 2011), or by the interaction of percolating melts/fluids with the peridotitic mantle (Rudnick and Ionov, 2007; Jeffcoate et al., 2007; Aulbach and Rudnick, 2009). Yakob et al. (2012) measured $D_{Li}^{(Ol\text{-}Cpx)}$ = 2.0 ± 0.2 at 1.5 GPa between 700-1100 °C, which is consistent with estimated P-T condition of the mantle xenoliths from the Thrace Basin in NW Turkey (Aldanmaz et al., 2005). Thus, the two times higher Li content in olivine than clinopyroxene would trigger Li diffusion from olivine to clinopyroxene and this diffusion process should have been ended when Li content in clinopyroxene was equilibrated to that in olivine (Seitz and Woodland, 2000). However, the large difference in Li contents of up to ~20 ppm between some clinopyroxenes (22.0 ppm) and olivines (2.11 ppm) (e.g. BK15-10) indicate disequilibrium fractionation. The record of such an extreme disequilibrium points toward ingress of Li-rich metasomatic melts or fluids, the preferential uptake of Li in pyroxenes over olivines and insufficient time to achieve equilibrium partitioning. Furthermore, the host magma-rock reaction leads to increasing Li concentrations with lighter δ^7Li in the rims (Jeffcoate et al., 2007; Rudnick and Ionov, 2007), whereas mantle metasomatism may result in reverse correlation (Tang et al., 2007). Generally, the studied pyroxenes, especially the orthopyroxenes, reveal lower Li content and heavier Li isotopic compositions in the rims (Figs. 7b, c). Thus, it is likely that mantle metasomatism (Zhang et al., 2010; Tang et al., 2011; Su et al., 2012, 2014a, b; Xiao et al., 2015; Gu et al., 2016), rather than the host magma, contributed dominantly to the observed disequilibrium of Li isotopic compositions in lithospheric mantle beneath the Thrace Basin. Although the orthopyroxene in sample BK15-10 shows Li enrichment in the rim (Fig. 7c), its heaviest Li isotopic composition still refutes the diffusion between minerals and/or host magma-rock.

5.3 Cryptic metasomatism and origin of metasomatized fluids/melts inferred

from Li contents and isotopic compositions

We propose that the mantle section represented by xenoliths studied here, were affected by partial melting. Because Li is a moderate incompatible element (Brenan et al., 1998a, b), it becomes depleted in the mantle upon partial melting. In equilibrated unmetasomatized 'normal' to slightly depleted mantle, Li contents of minerals decrease from 2 to 1 ppm with the following sequence of $Li_{Ol} > Li_{Opx} \geq Li_{Cpx}$ (Seitz and Woodland, 2000). Sample BK15-12, with low whole-rock Al_2O_3 content (0.66 wt.%, unpublished data), is the most refractory harzburgite and its low Li concentrations (0.15-0.30 ppm) in the orthopyroxenes also indicate high degree melt extraction. Furthermore, Os isotope ratios (0.1190) of sample BK15-12 indicate an ancient melt extraction possibly as old as Meso-Proterozoic (unpublished data), which is consistent with the previous study by Aldanmaz et al. (2012). However, Li concentrations in most pyroxenes from this study are significantly higher than in olivine, clearly manifesting melt/fluid-rock interaction (Figs. 5b, c). In addition, the clinopyroxene in the harzburgites and lherzolites reveal high Li contents and light δ^7Li values compared to olivine (Table S2; Fig. 5). The lack of secondary minerals and the very different Li signatures from 'normal' mantle are likely the result of cryptic metasomatism.

Additionally, a single metasomatic agent or event cannot explain the zonations of pyroxenes with light δ^7Li core and heavy rim compositions. The zonation in a single grain generally represents the effect of a relatively recent ingress of metasomatic agent(s) (Rudnick and Ionov, 2007), as displayed by the Li elemental and isotopic compositional profiles in orthopyroxene grains in our study (Fig. 6a). We argue that the orthopyroxene cores likely preserved the signatures (high Li content and light Li isotopes down to ~ -70‰) of a previous metasomatic overprint.

5.3.1 Fluid metasomatism

Subduction-related fluid-rock interaction is commonly characterized by whole-rock LILE (e.g. Pb, Sr, U) enrichment and HFSE (e.g. Nb, Ta) depletion (Morten and Obata 1990; Downes et al., 2001; Rampone and Morten 2001; Ionov, 2010). The progressive increase in Pb and depletion in Nb-Ta-Ti (Fig. 4) in most of our sample suggest the influx of slab-derived aqueous fluids. Fluids released from the subducted slab are variable in composition, depending on the mode of dehydration. However, because ^{7}Li preferentially enters the fluid phases (e.g. Huh et al., 2001; Kısakürek et al., 2004; Wunder et al., 2006, 2010), Li isotopic composition of the subducted slab would become progressively lighter during dehydration (e.g. Tomascak et al., 2002; Elliott et al., 2004, 2006). Dehydration also may significantly change the Li budgets of submarine vent fluids, which can be as low as ~ 1 ppm for marine sediment-starved hydrothermal systems or as high as ~ 40 ppm for marine sediment-hosted sites (Araoka et al., 2016).

Most pyroxene grains in the studied xenoliths have δ^{7}Li values that consistently become heavier from core to rim, with decreasing Li contents towards the rim (Figs. 7b, c), suggesting metasomatic overprint by a fluid or melt with low Li content and a heavy δ^{7}Li composition. The relatively low and homogeneous 'normal' mantle Li concentrations in olivines indicate negligible influence by the metasomatic agent(s) (Fig. 7a), reflecting the faster diffusion of Li in pyroxene compared to olivine (Parkinson et al., 2007; Rudnick and Ionov, 2007; Dohmen et al., 2010; Richter et al., 2014). The distinct zonation in the orthopyroxene compared to olivine and clinopyroxene implies that orthopyroxene is more sensitive and reactive to the metasomatic fluids or melts. The clinopyroxenes have light δ^{7}Li core compositions and heavier compositions in the rim. Li contents, however, show disordered

tendencies (Fig. 7c), implying a high variability of Li contents in the metasomatic agents. It is also suggested that metasomatism happened briefly before the entrainment of the xenoliths by the host lavas. Thus, olivines and the cores of the pyroxenes should be unaffected by such fluid metasomatism and therefore may record ancient metasomatic agents.

5.3.2 Silicate metasomatism

Contrary to the samples containing Li-poor orthopyroxenes that formed by partial melting and affected by a metasomatic agent with low Li contents, samples with pyroxenes that have high Li contents and light δ^7Li are remnants of a previous melt metasomatism (Fig. 5a). During metasomatism by silicate melts, Li preferentially enters the pyroxenes, whereby ^{6}Li is taken up faster by the crystal lattice, leading to kinetic isotopic fractionation and resulting in high Li contents and light Li isotopic compositions (Wagner and Deloule, 2007; Su et al., 2014a). The more sluggish reacting olivines are driven to heavier Li isotopic compositions, which is also in accordance with observations in this study. The Li concentration gradients cause diffusion to result in uniform Li content relative to δ^7Li of olivine in an individual sample, since it takes longer time for Li isotopes, compared to Li concentration to achieve compositional uniformity (Richter et al., 2014). This appears to be consistent with our data, pointing to the limited Li variations compared to the wide range of δ^7Li values in the olivines. Moreover, the olivines, which are apparently not much affected by the fluid metasomatism, show negative correlation between Fo contents and δ^7Li values, indicating the influence of silicate melts (Fig. 6a).

In this study, the metasomatic silicate melts most likely resulted in high Li contents and light δ^7Li compositions in the pyroxene cores. The lack of correlation between δ^7Li and major elements (Figs. 5c, 6b), is likely due to low degree of

melt-rock interaction and subsequent disturbance by fluids. Generally, olivine-websterite is thought to be product of silicate metasomatism and expected to show enrichment of Li in orthopyroxene (Su et al., 2014a). The olivine-websterite sample studied here has relatively low Li contents in orthopyroxene (1.52-1.78 ppm), with δ^7Li values ranging between -3.11 and 2.16‰ (Table S2), more likely reflect a cumulative origin and a production from previous stage of crystal fractionation process, which is evident by its depleted whole-rock LREE (Fig. 4c). Notably, the Li signatures of the silicate metasomatic agent have been recorded in the mineral cores and the fluid-related metasomatism lead to the observed Li zonation. Because of the lack of the major element zonation of minerals, we further conclude that Li isotope systematics are more sensitive to cryptic metasomatism.

5.4 Implications

The previous work on the mantle xenoliths from NW Turkey proposed a partial melting origin of the underlying Cenozoic lithospheric mantle, but did not discuss the processes of melts/rock interaction (Aldanmaz et al., 2005, 2012). Neither was the clarification of the mantle metasomatism, nor the origin of the fluids/melts constrained. The recycling of crustal materials needs to be considered and can give valuable insights into the evolution of Tethyan ocean. The low Li contents (< 1 ppm) in orthopyroxenes, together with normal-mantle bulk Li contents, indicates the low degree of melt/fluid-rock interaction, which has not been detected in previous studies. This also may explain the more depleted LREE patterns in the lherzolites compared to some harzburgites (Fig. 4).

The overall high δ^7Li values in olivine and extremely low δ^7Li values in pyroxenes (Fig. 5) suggest the importance of kinetic isotope fractionation during the interaction with silicate melts. The Y-depleted whole-rock signatures present in most

harzburgites from our study (Fig. 4) indicate that the melts originated in a garnet-bearing source (Green, 1982; Martin, 1999). Thus, the silicate melts derived by partial melting of the dehydrated eclogitic slab produced light δ^7Li pyroxenes and heavy olivines. The Triassic eclogites found in the southern Marmara Sea (Fig. 1; Okay et al., 1997, 2002) are a record of the subduction history of the Paleo-Tethys and confirm the existence of eclogites source in this region. After the silicate metasomatism events, which occurred during the Paleo-Tethys subduction, subduction-related fluids with low Li contents and heavy isotopic compositions may have been associated with the closure of the Intra-Pontide ocean, briefly before the eruption of the Miocene basalt in the Thrace Basin, NW Turkey.

6. Conclusions

We conclude that Li isotope systematics is very sensitive to cryptic metasomatism. The Li contents and isotopic compositions of minerals recorded in mantle xenoliths from the Thrace Basin, reveal disequilibrium distributions between coexisting minerals and extremely heterogeneous Li isotopic compositions. These features, together with whole rock trace element and mineral chemistry, demonstrate that these rocks have undergone a two-stage metasomatism: 1) a silicate melt metasomatism after melt extraction and 2) an overprint by fluids. The metasomatizing silicate melts are inferred to have been generated by partial melting of a dehydrated eclogitic slab during the subduction of the Paleo-Tethyan ocean, while the more recent metasomatic fluids are likely related to the closure of Intra-Pontide ocean.

Acknowledgements

We would like to thank Di Zhang, Yu Liu and Guo-Qiang Tang for their assistance with the electronic microprobe and SIMS analyses. The manuscript was

considerably improved by the thoughtful comments and suggestions of two anonymous reviewers. Patrick Asamoah Sakyi is thanked for his considerable time and efforts in helping with improving the English expression. This study was financially supported by National Natural Science Foundation of China (41522203 and 91755205), State Key Laboratory of Lithospheric Evolution (201701), and Youth Innovation Promotion Association, Chinese Academy of Sciences (2016067).

References

Aldanmaz E., 2012. Osmium isotope and highly siderophile element geochemistry of mantle xenoliths from NW Turkey: implications for melt depletion and metasomatic history of the sub-continental lithospheric mantle. International Geology Review 54, 799-815.

Aldanmaz E., Gourgaud A., Kaymakçı N., 2005. Constraints on the composition and thermal structure of the upper mantle beneath nw turkey: evidence from mantle xenoliths and alkali primary melts. Journal of Geodynamics 39, 277-316.

Aldanmaz E., Köprübaşı N., Gürer Ö.F., Kaymakçı N., Gourgaud A., 2006. Geochemical constraints on the Cenozoic, OIB-type alkaline volcanic rocks of NW Turkey: implications for mantle sources and melting processes. Lithos 86, 50-76.

Aldanmaz E., Pearce J.A., Thirlwall M.F., Mitchell J.G., 2000. Petrogenetic evolution of late Cenozoic, post-collision volcanism in Western Anatolia, Turkey. Journal of Volcanology and Geothermal Research 102, 67-95.

Aulbach S., Rudnick R.L., 2009. Origins of non-equilibrium lithium isotope fractionation in xenolithic peridotite minerals: examples from Tanzania. Chemical Geology 258, 17-27.

Araoka D., Nishio Y., Gamo T., Yamaoka K., Kawahata H., 2016. Lithium isotopic systematics of submarine vent fluids from arc and back- arc hydrothermal systems in the western Pacific. Geochemistry Geophysics Geosystems 17, 3835-3853.

Bodinier J.L., Vasseur G., Vernieres J., Dupuy C., Fabries J., 1990. Mechanisms of mantle metasomatism—geochemical evidence from the lherz orogenic peridotite. Journal of Petrology 31, 597-628.

Brenan J.M., Neroda E., Lundstrom C.C., Shaw H.F., Ryerson F.J., Phinney D.L., 1998a. Behaviour of boron, beryllium, and lithium during melting and crystallization: constraints from mineral-melt partitioning experiments. Geochimica et Cosmochimica Acta 62, 2129-2141.

Brenan J.M., Ryerson F.J., Shaw H.F., 1998b. The role of aqueous fluids in the slab-to-mantle transfer of boron, beryllium and lithium during subduction: experiments and models. Geochimica et Cosmochimica Acta 62, 3337-3347.

Chan L.H., Leeman W.P., You C.F., 1999. Lithium isotopic composition of central american volcanic arc lavas: implications for modification of subarc mantle by slab-derived fluids: correction. Chemical Geology 160, 255-280.

Chan L.H., Leeman W.P., You C.F., 2002. Lithium isotopic composition of Central American volcanic arc lavas: implications for modification of subarc mantle by slab-derived fluids: correction. Chemical Geology 182, 293-300.

Coogan L.A., Kasemann S.A., Chakraborty S., 2005. Rates of hydrothermal cooling of new oceanic upper crust derived from lithium-geospeedometry. Earth and Planetary Science Letters 240, 415-424.

Dawson J.B., 1984. Contrasting Types of Upper-Mantle Metasomatism?. Developments in Petrology 11, 289-294.

Dohmen R., Kasemann S.A., Coogan L., Chakraborty S., 2010. Diffusion of Li in olivine. Part I: Experimental observations and a multi species diffusion model. Geochimica et Cosmochimica Acta 74, 274-292.

Downes H., 2001. Formation and modification of the shallow sub-continental lithospheric mantle: a review of geochemical evidence from ultramafic xenolith suites and tectonically emplaced ultramafic massifs of western and central Europe. Journal of Petrology 42, 233-250.

Elliott T., Jeffcoate A., Bouman C., 2004. The terrestrial Li isotope cycle: light-weight constraints on mantle convection. Earth and Planetary Science Letters 220, 231-245.

Elliott T., Thomas, A., Jeffcoate, A., Niu, Y.L., 2006. Lithium isotope evidence for subduction enriched mantle in the source of mid-ocean-ridge basalts. Nature 443, 565-568.

Emre Ö., Erkal T., Tchepalyga A., Kazancl N., Keçer M., Ünay E., 1998. Neogene-Quaternary evolution of the Eastern Marmara Region, Northwest Turkey. Bulletin of the Mineral Research and Exploration Institute of Turkey 120, 119-145.

Ercan T., Satır M., Walter G.S., Yıldırım T., 1995. Biga yarımadası ile Gökçeada, Bozcaada ve Tavşan adalarındaki (KB Anadolu) Tersiyer volkanizmasının özellikleri. Maden Tetkik ve Arama Dergisi 117, 55-86.

Ersoy E.Y., Palmer M.R., Genç Ş.C., Prelević D., Akal C., Uysal İ., 2017. Chemo-probe into the mantle origin of the NW Anatolia Eocene to Miocene volcanic rocks: implications for the role of, crustal accretion, subduction, slab roll-back and slab break-off processes in genesis of post-collisional magmatism. Lithos 288, 55-71.

Flesch G.D., Anderson A.R., Svec H.J., 1973. A secondary isotopic standard for $^{6}Li/^{7}Li$ determinations. International Journal of Mass Spectrometry and Ion Physics 12, 265-272.

Gao Y., Snow J.E., Casey J.F., Yu J., 2011. Coolinginduced fractionation of mantle Li isotopes from the ultraslow-spreading Gakkel Ridge. Earth and Planetary Science Letters 301, 231-240.

Görür N., 1988. Timing of opening of the Black Sea basin. Tectonophysics 147, 247-262.

Görür N., Okay A.I., 1996. A fore-arc origin for the Thrace Basin, NW Turkey. Geologische Rundschau 85, 662-668.

Green T.H., 1982. Anatexis of mafic crust and high pressure crystallization of andesite. In: Thorpe R.S. (Ed.), Andesites. John Wiley and Sons, New York, pp. 465-487.

Green D.H., Wallace M.E., 1988. Mantle metasomatism by ephemeral carbonatite melts. Nature 336, 459-462.

Gürbüz A., Gürer Ö.F., 2008a. Anthropogenic affects on lake sedimentation process: a case study from Lake Sapanca, NW turkey. Environmental Geology 56, 299-307.

Gürbüz A., Gürer Ö.F., 2008b. Tectonic Geomorphology of the North Anatolian Fault Zone in the Lake Sapanca Basin (eastern Marmara Region, Turkey). Geosciences Journal 12, 215-225.

Gu X.Y., Deloule E., France L., Ingrin J., 2016. Multi-stage metasomatism revealed by trace element and Li isotope distributions in minerals of peridotite xenoliths from Allègre volcano (French Massif Central). Lithos 264, 158-174.

Harte B., 1983. Mantle peridotites and processes—the kimberlite sample. Continental Basalts and Mantle Xenoliths, 46-91.

Huh Y., Chan L.H., Edmond J.M., 2001. Lithium isotopes as a probe of weathering

processes: Orinoco River. Earth and Planetary Science Letters 194, 189-199.

Ionov D.A., Seitz H.M., 2008. Lithium contents and isotopic compositions in mantle xenoliths from subduction and intra-plate settings: mantle sources vs. eruption histories. Earth and Planetary Science Letters 266, 316-331.

Ionov D.A., 2010. Petrology of mantle wedge lithosphere: new data on supra-subduction zone peridotite xenoliths from the andesitic Avacha volcano, Kamchatka. Journal of Petrology 51, 327-361.

Jeffcoate A.B., Elliott T., Kasemann S.A., Ionov D., Cooper K., Brooker R., 2007. Li isotope fractionation in peridotites and mafic melts. Geochimica et Cosmochimica Acta 71, 202-218.

Kaymakçı N., Aldanmaz E., Langereis C., Spell T.L., Gürer Ö.F., Zanetti K.A., 2007. Late Miocene transcurrent tectonics in NW Turkey: evidence from palaeomagnetism and ^{40}Ar-^{39}Ar dating of alkaline volcanic rocks. Geological Magazine 144, 379-392.

Karacık Z., Tüysüz O., 2010. Petrogenesis of the Late Cretaceous Demirköy Igneous Complex in the NW Turkey: implications for magma genesis in the Strandja Zone. Lithos 114, 369-384.

Kısakürek B., Widdowson M., James R.H., 2004. Behaviour of Li isotopes during continental weathering: the Bidar laterite profile, India. Chemical Geology 212, 27-44.

Lundstrom C.C., Chaussidon M., Hsui A.T., Kelemen P., Zimmerman M., 2005. Observations of Li isotopic variations in the Trinity ophiolite: evidence for isotopic fractionation by diffusion during mantle melting. Geochimica et Cosmochimica Acta 69, 735-751.

Magna T., Wiechert U., Halliday A.N., 2006. New constraints on the lithium isotope

compositions of the Moon and terrestrial planets. Earth and Planetary Science Letters 243, 336-353.

Magna T., Ionov D.A., Oberli F, Wiechert U., 2008. Links between mantle metasomatism and lithium isotopes: Evidence from glass-bearing and cryptically metasomatized xenoliths from Mongolia. Earth and Planetary Science Letters 276, 214-222.

Marschall H.R., Pogge von Strandmann P.A.E., Seitz, H.M., Elliott T., Niu Y.L., 2007. The lithium isotopic composition of orogenic eclogites and deep subducted slabs. Earth and Planetary Science Letters 262, 563-580.

Martin H., 1999. Adakitic magmas: modern analogues of Archaean granitoids. Lithos 46, 411-429.

Menzies M.A., Rogers N., Tindle A., Hawkesworth C.J., 1987. Metasomatic and enrichment processes in lithospheric peridotites, an effect of asthenosphere-lithosphere interaction. In: Menzies M.A., Hawkesworth C.J. (Eds.), Mantle Metasomatism. Academic Press, London, pp. 313-361.

Menzies M.A., Xu Y.G., Zhang H.F., Fan W.M., 2007. Integration of geology, geophysics and geochemistry: a key to understanding the North China Craton. Lithos 96, 1-21.

McDonough W.F., Sun S.S., 1995. The composition of the Earth. Chemical Geology 120, 223-253.

Morten L., Obata M., 1990. Rare earth contents in the eastern Alpine peridotites, Nonsberg area Northern Italy. European Journal of Mineralogy 2, 643-653.

Nishio Y., Shunichi N., Yamamoto J., Sumino H., Matsumoto T., Prikhodko V.S., Arai, S., 2004. Lithium isotopic systematics of the mantle-derived ultramafic xenoliths: implications for EM1 origin. Earth and Planetary Science Letters 217, 245-261.

Ohta E., Dogan R., Batic H., Abe M., 1988. Geology and mineralization of Dereköy Porphyry copper deposits, northern Thrace, Turkey. Bulletin of the Geological Survey of Japan 39, 115-134.

Okay A.I., 2008. Geology of Turkey: a synopsis. Anschnitt 21, 19-42.

Okay A.I., Monod O., Monié P., 2002. Triassic blueschists and eclogites from northwest Turkey: vestiges of the Paleo-Tethyan subduction. Lithos 64, 155-178.

Okay A.I., Monié P., 1997. Early Mesozoic subduction in the Eastern Mediterranean: evidence from Triassic eclogite in northwest Turkey. Geology 25, 595-598.

Okay A.I., Satır M., Maluski H., Siyako M., Monie P., Metzger R., Akyüz S., 1996. Paleo- and Neo- Tethyan events in northwest Turkey: geological and geochronological constraints. In: Yin A., Harrison M. (Eds.), Tectonics of Asia. Cambridge University Press, Cambridge, 420-441.

Öngen S., 2000. Relationship between magnesian skarns and iron ore deposits at Dereköy, NW Turkey. Istanbul Yerbilimleri Dergisi 13, 63-75.

Ottolini L., Fèvre B.L., Vannucci R., 2004. Direct assessment of mantle boron and lithium contents and distribution by SIMS analyses of peridotite minerals. Earth and Planetary Science Letters 228, 19-36.

Parkinson I.J., Hammond S.J., James R.H., Rogers N.W., 2007. High-temperature lithium isotope fractionation: insights from lithium isotope diffusion in magmatic systems. Earth and Planetary Science Letters 257, 609-621.

Perinçek D., 1991. Possible strand of the North Anatolian fault in the Thrace Basin Turkey: an interpretation. AAPG Bulletin 75, 241-257.

Prouteau G., Scaillet B., Pichavant M., and Maury R., 2001. Evidence for mantle metasomatism by hydrous silicic melts derived from subducted oceanic crust. Nature 410, 197-200.

Rampone E., Morten L., 2001. Records of crustal metasomatism in the garnet peridotites of the Ulten Zone (Upper Austroalpine, Eastern Alps). Journal of Petrology 42, 207-219.

Richter F.M., Davis A.M., DePaolo D.J., Watson E.B., 2003. Isotope fractionation by chemical diffusion between molten basalt and rhyolite. Geochimica et Cosmochimica Acta 67, 3905-3923.

Richter F., Watson B., Chaussidon M., Mendybaev R., Ruscitto D., 2014. Lithium isotope fractionation by diffusion in minerals. Part I: Pyroxenes. Geochimica et Cosmochimica Acta 126, 352-370.

Rudnick R.L., Ionov D.A., 2007. Lithium elemental and isotopic disequilibrium in minerals from peridotite xenoliths from far-east Russia: product of recent melts/fluids-rock reaction. Earth and Planetary Science Letters 256, 278-293.

Rudnick R.L., Gao S., Ling W.L., Liu Y.S., McDonough W.F., 2004. Petrology and geochemistry of spinel peridotite xenoliths from Hannuoba and Qixia, North China craton. Lithos 77, 609-637.

Seitz H.M., Brey G.P., Lahaye Y., Durali S., Weyer S., 2004. Lithium isotopic signatures of peridotite xenoliths and isotopic fractionation at high temperature between olivine and pyroxenes. Chemical Geology 212, 163-177.

Seitz H.M., Woodland A.B., 2000. The distribution of lithium in peridotitic and pyroxenitic mantle lithologies—an indicator of magmatic and metasomatized processes. Chemical Geology 166, 47-64.

Şengör A.M.C., 1987. Tectonics of the Tethysides: orogenic collage development in a collisional setting. Annual Reviews of Earth and Planetary Sciences 15, 213-244.

Su B.X., Gu, X.Y., Deloule E., Zhang H.F., Li Q.L., Li X.H., Vigier N., Tang Y.J., Tang G.Q., Liu Y., Pang K.N., Brewer A., Mao Q., Ma Y.G., 2015. Potential

orthopyroxene, clinopyroxene and olivine reference materials for in situ Lithium isotope determination. Geostandards and Geoanalytical Research 39, 357-369.

Su B.X., Zhang H.F., Deloule E., Sakyi P.A., Xiao Y., Tang Y.J., Hu Y., Ying J.F., Liu P.P., 2012. Extremely high Li and low δ^7Li signatures in the lithospheric mantle. Chemical Geology 292, 149-157.

Su B.X., Zhang H.F., Deloule E., Vigier N., Hu Y., Tang Y.J., Xiao Y., Sakyi, P.A., 2014a. Distinguishing silicate and carbonatite mantle metasomatism by using lithium and its isotopes. Chemical Geology 381, 67-77.

Su B.X., Zhang H.F., Deloule, E., Vigier N., Sakyi P. A., 2014b. Lithium elemental and isotopic variations in rock-melts interaction. Chemie der Erde - Geochemistry 74, 705-713.

Su B.X., Zhang H.F., Sakyi P.A., Qin K.Z., Liu P.P., Ying J.F., Tang Y.J., Malaviarachchi, S.P.K., Xiao Y., Zhao X.M., Mao Q., Ma Y.G., 2010. Formation of melts pockets in mantle peridotite xenoliths from the Western Qinling (Central China): partial melting and metasomatism. Journal of Earth Science 21, 641-668.

Tang Y.J., Zhang H.F., Nakamura E., Moriguti T., Kobayashi K., Ying J.F., 2007. Lithium isotopic systematics of peridotite xenoliths from Hannuoba, North China Craton: implications for melts/rock interaction in the considerably thinned lithospheric mantle. Geochimica et Cosmochimica Acta 71, 4327-4341.

Tang Y.J., Zhang H.F., Nakamura E., Ying J.F., 2011. Multistage melts/fluids-peridotite interactions in the refertilized lithospheric mantle beneath the North China Craton: constraints from the Li-Sr-Nd isotopic disequilibrium between minerals of peridotite xenoliths. Contributions to Mineralogy and Petrology 161, 845-861.

Tang Y.J., Zhang H.F., Ying J.F., Su B.X., 2013. Widespread refertilization of cratonic

and circum-cratonic lithospheric mantle. Earth-Science Reviews, 118, 45-68.

Tomascak P.B., 2004. Developments in the understanding and application of lithium isotopes in the earth and planetary sciences. Reviews in Mineralogy and Geochemistry 55, 153-195.

Tomascak P.B., Magna T., Dohmen R., 2016. Advances in Lithium Isotope Geochemistry. Springer International Publishing.

Tomascak P.B., Tera F., Helz R.T., Walker R.J., 1999. The absence of lithium isotope fractionation during basalt differentiation: new measurements by multi-collector sector ICP-MS. Geochimica et Cosmochimica Acta 63, 907-910.

Vlastélic I., Koga K., Chauvel C., Jacques G., Telouk P., 2009. Survival of lithium isotopic heterogeneities in the mantle supported by HIMU-lavas from Rurutu Island, Austral Chain. Earth and Planetary Science Letters 286, 456-466.

Wagner C., Deloule E., 2007. Behaviour of Li and its isotopes during metasomatism of French Massif Central lherzolites. Geochimica et Cosmochimica Acta 71, 4279-4296.

Wilkinson J.F.G., Maitre R.W.L., 1987. Upper mantle amphiboles and micas and TiO_2, K_2O, and P_2O_5 concentrations and 100 Mg/(Mg+Fe^{2+}) ratios of common basalts and andesites: implications for modal mantle metasomatism and undepleted mantle compositions. Journal of Petrology 28, 37-73.

Woodland A.B., Seitz H.M., Yaxley G.M., 2004. Varying behaviour of Li in metasomatised spinel peridotite xenoliths from western Victoria, Australia. Lithos 75, 55-66.

Wunder B., Meixner A., Romer R.L., Heinrich W., 2006. Temperature-dependent isotopic fractionation of lithium between clinopyroxene and high-pressure hydrous fluids. Contribution to Mineralogy and Petrology 151, 112-120.

Wunder B., Deschamps F., Watenphul A., Guillot S., Meixner A., Romer R.L., Wirth R., 2010. The effect of chrysotile nano-tubes on the serpentine-fluid Li-isotopic fractionation. Contribution to Mineralogy and Petrology 159, 781-790.

Yakob J.L., Feineman M.D., Deana Jr. J.A., Eggler D.H., Penniston-Dorland S.C., 2012. Lithium partitioning between olivine and diopside at upper mantle conditions: an experimental study. Earth and Planetary Science Letters 329-330, 11-21.

Yilmaz Y., Polat A., 1998. Geology and evolution of the thrace volcanism Turkey. Acta Vulcanologica 10, 293-303.

Xiao Y., Zhang H.F., Deloule E., Su B.X., Tang Y.J., Sakyi P.A., Hu Y., Ying J.F., 2015. Large Lithium Isotopic Variations in Minerals from Peridotite Xenoliths from the Eastern North China Craton. The Journal of Geology 123, 79-94.

Zhang H.F., Deloule E., Tang Y.J., Ying J.F., 2010. Melts/rock interaction in remains of refertilized Archean lithospheric mantle in Jiaodong Peninsula, North China Craton: Li isotopic evidence. Contributions to Mineralogy and Petrology 160, 261-277.

Zhang H.F., Goldstein, S.L., Zhou, X.H., Sun, M., Zheng, J.P., Cai, Y., 2008. Evolution of subcontinental lithospheric mantle beneath eastern China: Re-Os isotopic evidence from mantle xenoliths in Paleozoic kimberlites and Mesozoic basalts. Contributions to Minerology and Petrology 155, 271-293.

Zhang H.F., Sun M., Zhou X.H., Fan W.M., Zhai M.G., Ying J.F., 2002. Mesozoic lithosphere destruction beneath the North China Craton: evidence from major-, trace-element and Sr-Nd-Pb isotope studies of Fangcheng basalts. Contributions to Mineralogy and Petrology 144, 241-254.

Figures:

Figure 1. (a) The tectonic outline of Turkey and the eastern Mediterranean area (modified after Okay et al., 1996). (b) Simplified geological map of NW Turkey, showing the localities of xenolith-bearing Cenozoic basalts (modified after Ersoy et al., 2017). NAFZ: North Anatolian Fault Zone.

Figure 2. Petrography of the mantle-derived xenoliths from NW Turkey. (a) Sharp contact of peridotite with host basalt. (b) Medium-grained harzburgite (sample BK15-12). (c) Medium-grained lherzolite (sample BK15-14). (d) Medium-grained olivine-websterite (sample BK15-15). (e) Olivine kink band in harzburgite BK15-7. (f) Medium-grained silicate minerals with fined-grained spinel in olivine-websterite BK15-15. (g) Coarse-grained and granular olivine with medium-grained pyroxenes and spinel in lherzolite BK15-19. (h) Undulated boundaries between the medium-grained major minerals in harzburgite BK15-11. Ol, olivine; Cpx, clinopyroxene; Opx, orthopyroxene; Sp, spinel.

Figure 3. Mg# versus Al_2O_3 correlation diagrams for orthopyroxenes (a) and clinopyroxenes (b) in mantle xenoliths from NW Turkey.

Figure 4. Chondrite-normalized rare earth element and primitive mantle-normalized trace element patterns for mantle xenoliths from NW Turkey. The chondrite and primitive mantle values are from McDonough and Sun (1995). Symbols are same in Fig. 3.

Figure 5. δ^7Li versus Li contents correlation diagrams for (a) olivines, (b)

orthopyroxenes and (c) clinopyroxenes in mantle xenoliths from NW Turkey. Normal mantle values are from Seitz et al. (2004), Magna et al. (2006), Jeffcoate et al. (2007) and Tomascak et al. (2008). Symbols are same in Fig. 3. Harz.: harzburgite; Lhz.: lherzolite.

Figure 6. Correlation diagrams of δ^7Li versus (a) Fo contents in olivines, (b) Al_2O_3 in orthopyroxenes and (c) CaO in clinopyroxnes in mantle xenoliths from NW Turkey. Symbols are same in Fig. 3

Figure 7. Profiles of Li contents and isotopic compositions of orthopyroxenes (Opx) and clinopyroxenes (Cpx) of the mantle xenoliths from NW Turkey. Harz.: harzburgite; Lhz.: Lherzolite.

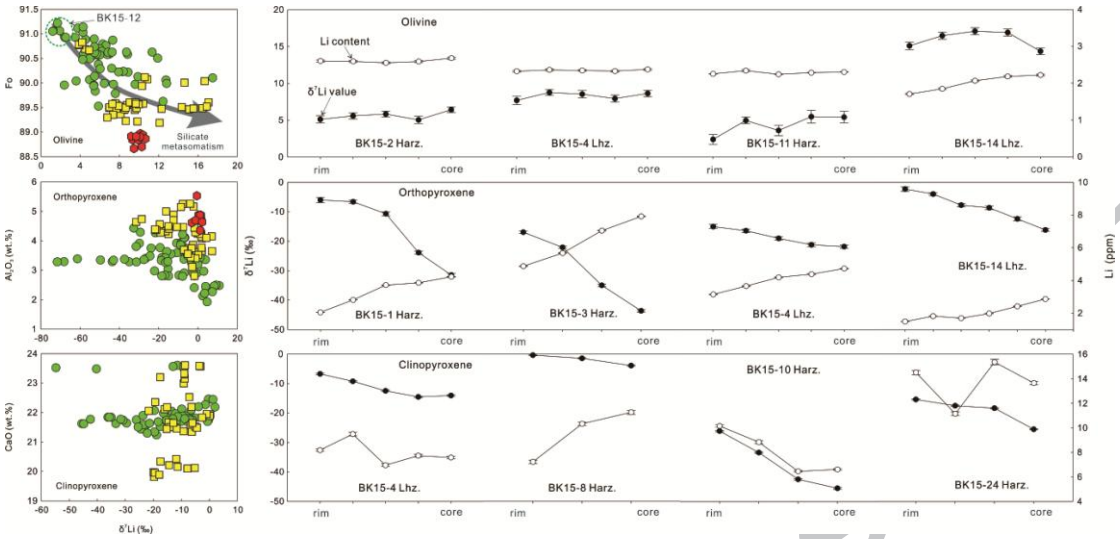

Highlights

(1) in-situ Li isotope measurement of olivine, orthopyroxene and clinopyroxene of a suite of mantle xenoliths from NW Turkey; (2) silicate melt metasomatism and recent fluid metasomatism revealed by Li isotope systematics; (3) silicate melts from dehydrated slab and subduction-related fluids inferred as metasomatic melts and fluids; (4) sensitivity of Li isotope systematics to cryptic metasomatism.